Electronic Supplementary Material (ESI) for CrystEngComm.

Electronic supplementary information

Non-classical crystal growth on the hydrophobic substrate: learning from bivalve nacre

Xin Feng*[a], Ruohe Gao[a], Rize Wang[a], Gangsheng Zhang[a]

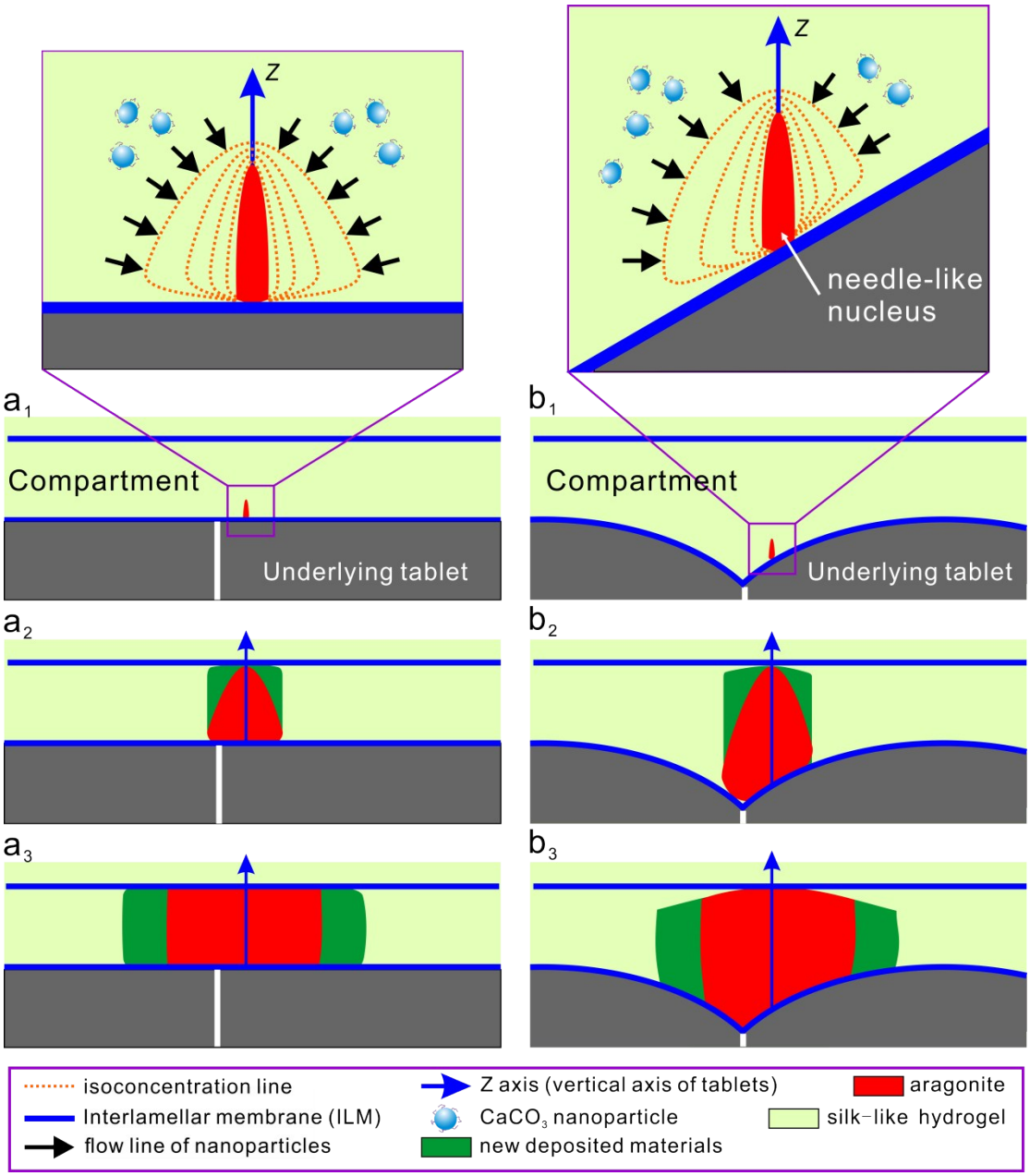

Fig. S1. Schematic illustration of the growth environment and size-dependent shapes of the nacreous tablets in flat (a1 - a3) and domed (b1 - b3) nacre of bivalves (in cross section). The growth environment of the tablet is according to the description of Addadi et al.[3], Checa et al.[4], Asenath-Smith et al.[5], and Marie et al.[6]. The concentration fields around the needle-like crystals are adapted from Raz et al.[7], Emsellem and Tabeling[8], and Sawada and Takemura[9]. The shape evolution of the tablets is based on the observation of this work.

Please note that:

(1) Based on the previous studies[10–12], the tablets are assumed to grow in the compartments between two adjacent ILMs with pores, which are permeable to the depositing materials (such as Ca^{2+}, CO_3^{2-}, and nanoparticles). In addition, the compartments are full of silk-like proteins hydrogel[3], which facilitate the diffusion-limited growth of the tablets[5].

(2) Based on the previous studies[3,10,11] and this work, the general growth process of the tablets includes four stages: I) nucleation stage, when the tablets nucleate on the underlying ILM or mineral bridges and appear as needles or rods (Fig. S1 a1 and b1); II) early growth stage, when they grow both vertically and laterally and appear as pyramids (Fig. S1 a2 and b2), until they meet the overlying ILM; III) middle growth (shape transition) stage, when they transition in shape from pyramids to prisms through intermediate shape of frustums; IV) late growth stage, when they grow only laterally and so develop a characteristic top surface until they meet other tablets (Fig. S1 a3 and b3).

(3) It has been well established that the diffusion field (isoconcentration lines) around a needle-like crystal (growing from water solution) is similar in shape to a family of paraboloids of revolution (Ivantsov diffusion field)[7–9], as shown in the insets of Fig. S1 a1 and b1. However, for the nacreous tablets, the isoconcentration lines should converge to their bottom due to the hydrophobicity of the ILM, based on the observation that the tablets always show a high contact angle on the ILM (Fig. 2 in the article).

(4) During the early growth stage, for the domed tablets studied in this work, their asymmetric shape can be attributed to the asymmetric diffusion field at the downslope and upslope side (inset of Fig. S1 b1), which arises from that the central axis (Z-axis) of the tablets is inclined to the substrate. Therefore, during growth, the flux of the depositing materials (such as nanoparticles) to the tablet's surface is obviously greater at the downslope side than at the upslope side. On the contrary, for the flat tablets, their shape is always symmetrical due to that their z-axis is perpendicular to the substrate (inset of Fig. S1 a1).

(5) During the middle growth stage, the shape transition from pyramids to prisms through frustums may be attributed to the increasing elastic strain energy induced by the occlusion of the biopolymers into the crystal lattices of the tablets[13]. As detailed before[14–16], during growth of a strained crystal, the new materials are preferentially deposited on the less strained surface of the crystal. Therefore, for the pyramidal tablets, as their top location is less strained than the bottom, the new nanoparticles are preferentially deposited around their top, which results in the shape transition of the tablets (Fig. S1 a2 and b2).

(6) During the late growth stage, the vertical growth of the tablet may be attributed to the space confinement by the ILMs (Fig. S1 a3 and b3), as detailed previously (e.g. Addadi et al., 2006).

(7) During all growth stages, the tablets (in top views) usually exhibit incomplete or complete hexagonal crystallographic shapes of aragonite (Fig. 1a), indicating that the growth of the tablets is always controlled to some extent by the crystallography of aragonite.

(8) During all growth stages, the tablets (in side or oblique views) always show a high contact angle with the ILM substrate and overhang attachment pattern of nanoparticles (Fig. 2), indicating that the hydrophobicity of the ILM is one of the factors affecting the growth of the tablets.

In summary, the crystallization process (growth) of the nacreous tablets is more complex than

might be expected, and influenced by many factors. They may work cooperatively or independently to regulate the nacre formation. Therefore, it is a long-standing challenge to fully understand the crystallization mechanism of the nacreous tablets. Finally, for simplicity, the above descriptions are reproduced as table S1.

Table S1 Possible factors influencing the crystallization process of the nacreous tablets based on the previous and present works (the detailed description is presented in the notes to Figure S4)

Factors		Growth stage	Evidence	Reference
Crystallography of aragonite, Hydrophobicity of the substrate (ILM)	Diffusion-limited growth regime	Early	Growth in the medium of Silk-like protein hydrogel. Pyramidal shape consistent with that predicted by the Ivantsov diffusion field	3,5,7–9
	Elastic strain energy, space confinement	Middle	The height of the tablets corresponding to that of the compartment. the new nanoparticles to preferentially deposit around the top part of the tablets	13–16
	space confinement	Late	The height of the tablets corresponding to that of the compartment.	3

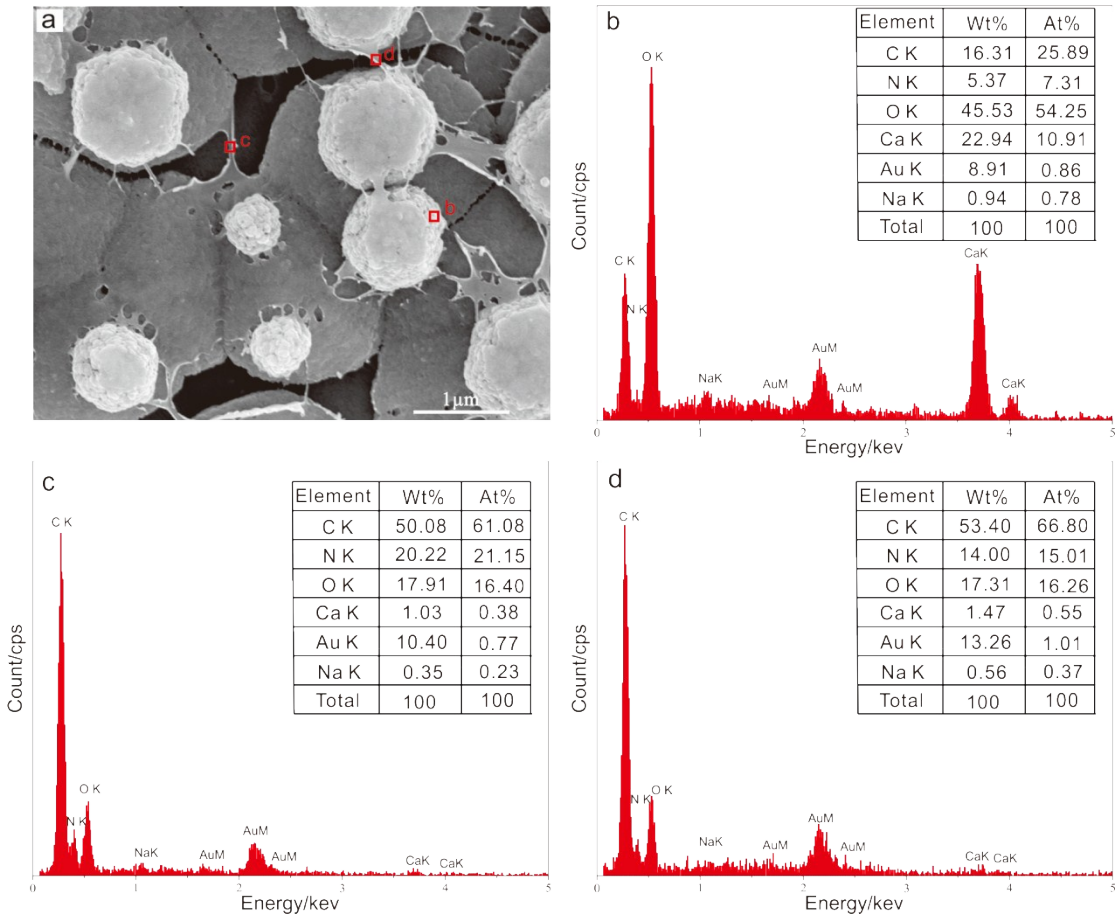

Fig. S2. (a)Top view of the inner surface of nacre (corresponding to the Fig. 1a in the article) and related energy dispersive X-ray (EDS) spectrums (b-d). The spectrums of (b), (c) and (d) corresponding to the red rectangle areas b, c and d in (a), respectively.

Please note that:

(1) The nacre consists of two components: more than 95wt.% aragonite tablets and small biopolymers[1,2].

(2) Under SEM (Fig. S2a), the red rectangle areas c and d are located on the base and top ILM (interllamellar membrane) of the tablet, respectively, while b on the growing aragonite nanoparticles.

(3) The spectra (c) and (d) indicate that base (i.e. growth substrate) and top (i.e. cover) ILM of the tablet mainly consist of element C, N, O, implying that they are of the biopolymer membranes (organic materials).

(4) The spectra (b) indicates that the growing aragonite nanoparticles mainly consist of the element C, O, Ca, but with minor N, implying that the tablet is mainly composed of $CaCO_3$ and a small amount of biopolymers.

(5) All EDS spectra were obtained with a field emission SEM (Hitachi, SU8020) at 10KV, which is attached with an EDS analyser (Oxford, X-MAX 80). The element Au is from the gold film coated on the samples, for the SEM observation. In addition, the surface membranes were broken and damaged due to the shrinkage during drying and gold-coating of the samples.

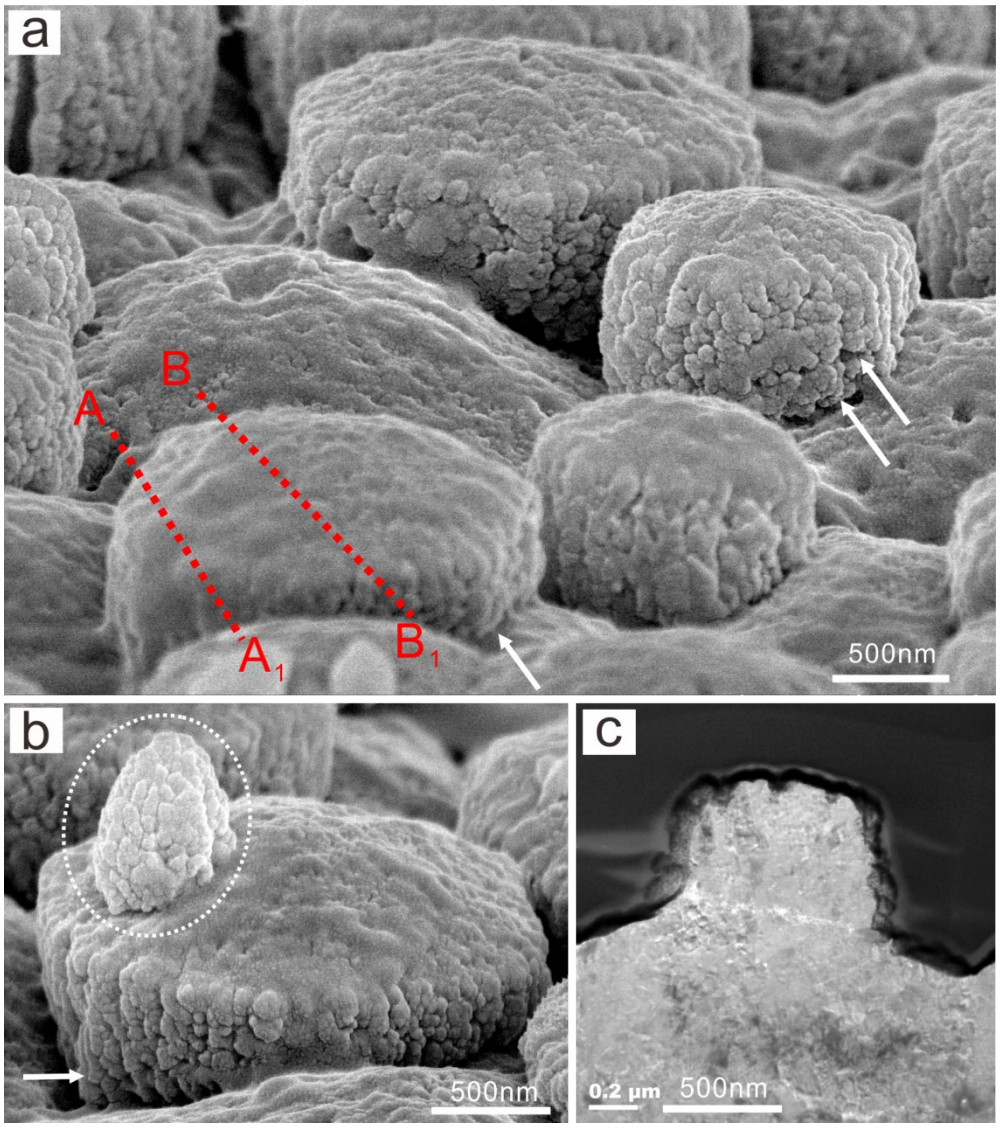

Fig. S3. (a)-(b) SEM images of the prism-like tablets with various sizes (in perspective view). (c) Bright-field TEM image of the prism-like tablet cut perpendicular to the inner surface of nacre, which is the enlarged view of the middle growing tablet in Figure 3a of the article.

Please note that:

(1) The prism-like tablet is characterized by having six lateral surfaces vertical to the inner surface of nacre, one convex top surface, and irregular concave bottom surfaces. Therefore, for a same tablet, their shape and size in vertical sections may vary greatly, which depend on the location and direction cut through the samples (such as cut through the line AA1 and BB1 in (a). Nevertheless, the lateral surfaces of any vertical sections are usually vertical (as shown in (c)).

(2) The prism-like tablet also show the phenomena of overhang attachment of nanoparticles and high contact angles (white arrows in (a) and (b)), which, however, are less significant as compared with the pyramid-like tablets.

(3) On the top of a fully developed tablet, the new generation of tablets is usually observed to occur (white circle in (b)).

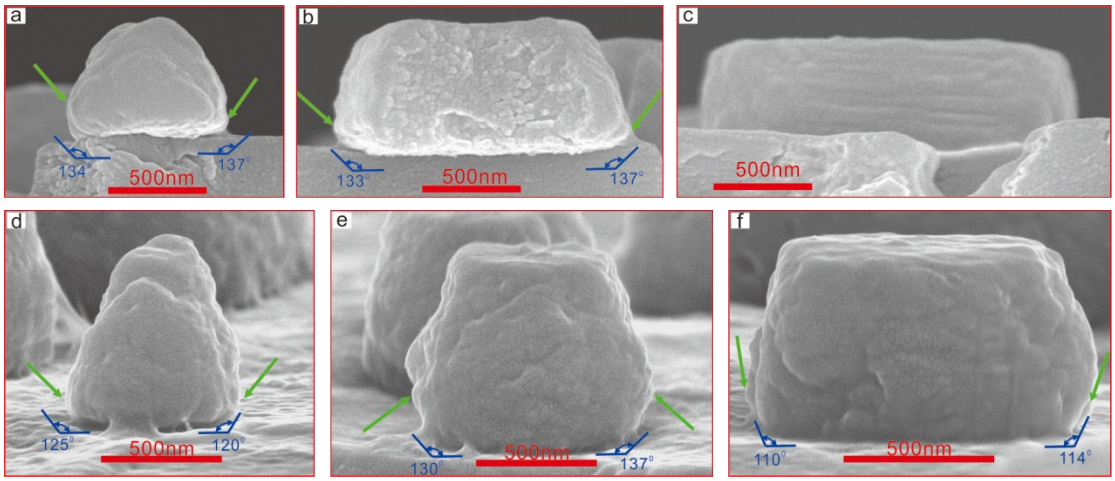

Fig. S4. Side-views of the nacreous tablets from bivalve *Modiolus kurilensis* (a-c) and *Hyriopsis cumingii* (d-f). (a, d) Pyramid-like. (b, e) Frustum-like. (c, f) Prism-like. θ： apparent contact angle between the tablet and substrate.

Please note that:

(1) The substrates are nearly flat and parallel to the inner surface of nacre.

(2) The tablets are nearly symetrical about their central axis.

(3) The apparent contact angle is unusually high (>90^0);

(4) Some nanoparticles exhibit a surprising overhanging attachment pattern (as green arrows).

Reference

1 J. Kong, C. Liu, D. Yang, Y. Yan, Y. Chen, Y. Liu, G. Zheng, L. Xie and R. Zhang, *CrystEngComm*, 2019, **21**, 1250–1261.

2 F. Marin, N. Le Roy, B. Marie, P. Ramos-Silva, S. Wolf, S. Benhamada, N. Guichard and F. Immel, *Key Eng. Mater.*, 2014, **614**, 52–61.

3 L. Addadi, D. Joester, F. Nudelman and S. Weiner, *Chem. - A Eur. J.*, 2006, **12**, 980–987.

4 A. G. Checa, J. H. E. Cartwright, B. Escribano and I. Sáinz-Díaz, *Mater. Res. Soc. Symp. Proc.*, 2008, **1094**, 92–97.

5 E. Asenath-Smith, H. Li, E. C. Keene, Z. W. Seh and L. A. Estroff, *Adv. Funct. Mater.*, 2012, **22**, 2891–2914.

6 B. Marie, C. Joubert, A. Tayalé, I. Zanella-Cleón, C. Belliard, D. Piquemal, N. Cochennec-Laureau, F. Marin, Y. Gueguen and C. Montagnani, *Proc. Natl. Acad. Sci. U. S. A.*, 2012, **109**, 20986–20991.

7 E. Raz, S. G. Lipson and E. Polturak, *Phys. Rev. A*, 1989, **40**, 1088–1095.

8 V. Emsellem and P. Tabeling, *Epl*, 1994, **25**, 277–283.

9 T. Sawada, K. Takemura, K. Shigematsu, S. I. Yoda and K. Kawasaki, *Phys. Rev. E*, 1995, **51**, 3834–3838.

10 T. E. Schäffer, C. Ionescu-Zanetti, R. Proksch, M. Fritz, D. A. Walters, N. Almqvist, C. M. Zaremba, A. M. Belcher, B. L. Smith, G. D. Stucky, D. E. Morse and P. K. Hansma, *Chem. Mater.*, 1997, **9**, 1731–1740.

11 A. Y. M. Lin, P. Y. Chen and M. A. Meyers, *Acta Biomater.*, 2008, **4**, 131–138.

12 A. G. Checa, J. H. E. Cartwright and M. G. Willinger, *J. Struct. Biol.*, 2011, **176**, 330–339.

13 E. Zolotoyabko, *Adv. Mater. Interfaces*, , DOI:10.1002/admi.201600189.

14 D. E. Jesson, G. Chen, K. M. Chen and S. J. Pennycook, *Phys. Rev. Lett.*, 1998, **80**, 5156–5159.

15 J. Johansson and W. Seifert, *J. Cryst. Growth*, 2002, **234**, 132–138.

16 C. Lofton and W. Sigmund, *Adv. Funct. Mater.*, 2005, **15**, 1197–1208.

17 S. Sang and X. Yang, *PeerJ*, 2018, **6**, e4333.

18 N. Kondekar, M. G. Boebinger, M. Tian, M. H. Kirmani and M. T. McDowell, *ACS Nano*, 2019, **13**, 7117–7126.